Electrodynamics of the spin-density-wave ground state: Optical experiments on (TMTSF)$_2$PF$_6$

S. Donovan, Yong Kim, L. Degiorgi,† M. Dressel, and G. Grüner

Department of Physics and Solid State Science Center, University of California, Los Angeles, California 90024-1547

W. Wonneberger

Abteilung für Mathematische Physik, Fakultät für Naturwissenschaften, Universität Ulm, D-89081 Ulm, Germany

(Received 8 June 1993)

Conductivity measurements are reported in the organic linear-chain compound (TMTSF)$_2$PF$_6$, in both the metallic and spin-density-wave states. The components of the complex conductivity were established by measurements in the radio-frequency, micro- and millimeter wave, and infrared spectral ranges. At temperatures above the spin-density-wave transition, a Drude-like metallic behavior was found together with a temperature-independent feature at higher frequencies. An observed Drude scattering rate of 3 cm^{-1} was found, placing the material well into the clean limit. In the spin-density-wave state, the low field dc resistivity shows an activated behavior similar to a standard semiconductor with a gap value $2\Delta/k_B \approx 45$ K. The ac response shows a strong frequency dependence, and most importantly, we observe two subgap modes: a very broad one in the radio frequency range, due to internal deformations of the spin density wave, and a narrow mode near 0.1 cm^{-1}, which we interpret as the response of the $q=0$ phason. Furthermore, as expected for a material in the clean limit, we do not see evidence for a single particle gap in the infrared spectral range. In this paper, we will compare our experimental results with the various models of spin-density-wave dynamics and comment on the current status of the understanding of the dynamical response of spin density waves.

I. INTRODUCTION

The electrodynamics of materials exhibiting various broken symmetry ground states, such as superconductors or charge density waves (CDW's),[1] is by now thoroughly explored and the main features of the frequency-dependent conductivity $\hat{\sigma}(\omega) = \sigma_1(\omega) + i\sigma_2(\omega)$, where $\sigma_1(\omega)$ and $\sigma_2(\omega)$ represent the real and imaginary parts of the response, are well understood.

While the collective mode is centered at zero frequency with a vanishing spectral width for a superconductor at $T = 0$ K, the interaction between the CDW and lattice imperfections shifts the oscillator strength to finite frequencies, with the center (pinning) frequency usually well below the single particle gap frequency $2\Delta/h$. For a superconductor, both collective mode and single particle excitations are possible and the relative strength of each depends on the ratio ξ_0/ℓ, where ξ_0 is the coherence length and ℓ is the mean free path. On the other hand, for CDW's the collective mode spectral weight depends on m_b/m^*, where m^* is the dynamical mass associated with the CDW and m_b the band mass. The remaining spectral weight, $1 - m_b/m^*$, is associated with single particle transitions across the gap and due to the prominent role played by the phonons, $m_b/m^* \ll 1$, and most of the spectral weight resides with the single particle excitations. Generally the two modes are well separated and each can be observed by measuring the conductivity $\sigma_1(\omega)$ over a broad spectral range. With transition

temperatures on the order of 100 K, mean field theory gives $2\Delta/h$ of the order of 100–1000 cm^{-1}, in the infrared range of frequencies, while the pinned mode resonance usually occurs in the millimeter wave spectral range in nominally pure specimens.[1–3]

Much less is known about the dynamics of the spin-density-wave (SDW) ground state which develops at low temperatures in several organic linear-chain compounds. The prime example is bis-(tetramethyltetraselanafulvalene)-hexaflourophosphate, (TMTSF)$_2$PF$_6$, which undergoes a metal-insulator transition at $T_{\text{SDW}}=12.0$ K. The state below T_{SDW} is weakly magnetic as evidenced by static magnetic susceptibility and antiferromagnetic resonance measurements.[4–6] In addition, NMR (Refs. 7 and 8) and μSR (Ref. 9) measurements clearly establish that the ground state is represented by a periodic modulation of the electronic spin density

$$\mathbf{S}(\mathbf{r}) = \mathbf{S}_1 \cos(\mathbf{Q} \cdot \mathbf{r} + \phi), \tag{1}$$

where $\mathbf{S}_1$ and ϕ are the amplitude and phase of the collective mode and $\mathbf{Q}$ is the nesting vector. The SDW period is incommensurate with the underlying lattice,[7,8,10–12] in agreement with nesting due to the two dimensional band structure.[13]

Although it is a magnetically ordered ground state, it has been shown theoretically[14] that an externally applied electric field couples directly to the SDW. The resulting ac or dc currents correspond to either an oscillatory or translational motion of the collective mode. The

SDW couples to magnetic impurities and recent calculations also suggest a significant coupling to nonmagnetic impurities.[15] These results imply that the collective mode response should occur at finite frequencies,[16-19] as seen previously in several CDW compounds. However, in contrast to the CDW ground state, the SDW state is formed as a consequence of electron-electron interactions, and the effective mass of the condensate, m^*, is expected to be the same as m_b.[14,17,19,20] This prediction has important consequences for the various contributions (collective mode and single particle) to the total spectral weight and will be discussed at some length later.

Early experiments[21] on $(TMTSF)_2PF_6$ in the SDW state indicated a nonlinear response in small applied dc fields while measurements at 9 GHz (Refs. 22-25) indicated a substantial enhancement of the low frequency conductivity in the spectral range well below the single particle gap. It was argued that both the nonlinear and frequency-dependent transport reflected the contribution of the SDW. However, microcracks which developed in the samples upon cooling prevented the observation of the expected sharp onset for nonlinear conduction. Improvements in the contact techniques, together with the use of carefully controlled cooling rates, allowed for the first unambiguous measurement of the threshold field E_T for SDW conduction.[26,27] These measurements were quickly followed by a wide variety of experiments providing further information about the SDW. Current oscillations, Shapiro steps, memory effects, and field hysteresis have all been observed[28-30] and recent NMR measurements[31,32] clearly show the narrowing of the proton linewidth above E_T, due to the motion of the SDW.

Further studies on the frequency dependence of the conductivity[33] have shown the presence of a low lying mode which is centered near 3 GHz with a strength which is more than two orders of magnitude smaller than expected from simple arguments based on spectral weight conservation. The large reduction of the spectral weight of this mode has been independently confirmed by measurements of the dielectric constant in the radio-frequency range.[34]

Several models or explanations have been proposed to account for the strongly reduced spectral weight in the SDW state. These models naturally fall into the following three categories: The observed resonance is not the SDW phason, the SDW mass is significantly larger than the band mass, or the number of relevant excitations of the SDW is small. Here we will briefly summarize some of these ideas and their implications. It has been suggested[35] that the observed mode may be due to the internal deformations[36] ($q \neq 0$) of the SDW. In this case, the pinned mode resonance, which should be at frequencies well above the spectral range where the modes due to internal deformations occur, would most likely be above the gap, i.e., $\hbar\omega_0 > 2\Delta$. It was also proposed[37] that impurities in the sample may lead to a mixing of the $q = 0$ magnon and phason modes. Such a system would display a low lying resonance due to a magnon excitation at the antiferromagnetic resonance frequency. On the other hand, an enhanced effective mass, due to a finite cou-

pling to the phonons, would strongly reduce the spectral weight of the SDW.[38,39] However, this can be ruled out, as the accompanying lattice distortion has not been found in the SDW state.[40] Another possible explanation[41] is that, as in a superconductor, long range Coulomb forces shift the spectral weight away from the pinning frequency ω_0 up to the plasma frequency ω_p. In a translationally invariant system, such a model, based on the so-called Anderson-Higgs mechanism,[42] would apply only to the longitudinal mode ($q \parallel E$) leaving the transverse mode ($q \perp E$), as sampled with optical measurements, unaffected. However, the transverse and longitudinal modes may be mixed due to anisotropy effects and interactions with the randomly situated impurities. Finally, bound states, due to either impurities[15] or commensurability effects,[43] could give rise to a distribution of subgap resonances. Such resonances would be expected to have a large spectral weight and therefore (due to the conservation of the total spectral weight) these states would strongly reduce the strength of the SDW phason.

In this paper we report on experimental results of the frequency-dependent conductivity $\hat{\sigma}(\omega)$. Experimental results from a variety of different techniques were combined in order to evaluate the electrodynamic response of $(TMTSF)_2PF_6$ over a broad spectral range, from dc up to optical frequencies. We also present a simple analysis of the experimental findings, in terms of a Drude response ($T > T_{SDW}$) and a harmonic oscillator response ($T < T_{SDW}$). Finally, we compare our results with several different models and find both a qualitative and quantitative agreement within an extended Fukuyama-Lee-Rice model. Parts of our results have been previously reported.[33,44-46]

II. EXPERIMENTAL TECHNIQUES AND RESULTS

Several different techniques have been employed in order to explore the electrodynamics of both the normal and the SDW states of $(TMTSF)_2PF_6$. The low frequency spectral range was investigated using standard ac techniques, resonant cavities were employed in the micro- and millimeter wave spectral range, and optical methods were used in the infrared spectral range. The data obtained with each technique were combined to determine the $\hat{\sigma}(\omega)$ over a broad spectral range. Before discussing the experimental results we will describe each of the experimental techniques.

All the measurements reported here were made on crystals of $(TMTSF)_2PF_6$ prepared by the standard electrochemical growth method.[47] The dc resistivity of a typical sample is shown together with its logarithmic derivative in Fig. 1. A metal-insulator transition is clearly visible near $T_{SDW}=12.0$ K, with the sharpness of the logarithmic derivative, as shown in the inset of Fig. 1, indicative of the high crystal quality. An activated behavior ($\sigma_1 = \sigma_0 e^{-\Delta/k_B T}$) is observed below T_{SDW}, with an activation energy $2\Delta/k_B=46$ K, in excellent agreement with the predictions of a weak-coupling mean field theory ($2\Delta = 3.5 k_B T_c$).
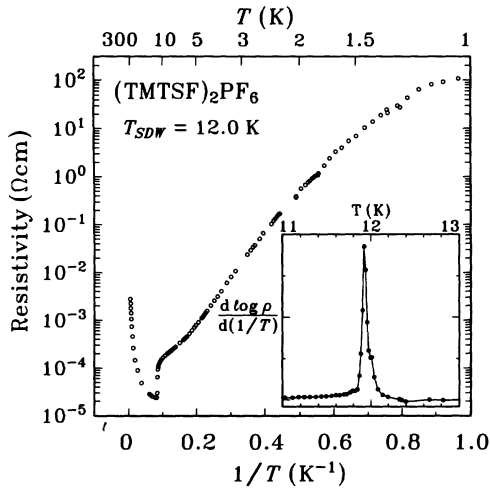
FIG. 1. The dc resistivity vs inverse temperature for a typical sample of $(TMTSF)_2PF_6$. From the slope of the curve one obtains a gap $2\Delta/k_B \approx 46$ K. The logarithmic derivative is shown in the inset.

A. Experiments in the radio-frequency spectral range

In the frequency range below 1 MHz, two different techniques were used to extract $\hat{\sigma}(\omega)$. In both cases, measurements were made in a four probe configuration with 5 μm Au wires attached with Ag paint to a conducting Ag pad evaporated on the surface of the sample. Each pad wrapped completely around the sample and both ends were covered with evaporated Ag to maximize the homogeneity of the current injection. A schematic of the experimental setup used in the audio-frequency range is shown in Fig. 2. A large serial load resistance $(R_{\text{load}} \gg R_{\text{sample}})$ was used to ensure that the experiments were carried out in a current controlled configuration. Furthermore, to guarantee the applicability of linear response theory, care was taken that the electric field was always well below the threshold field for nonlin-
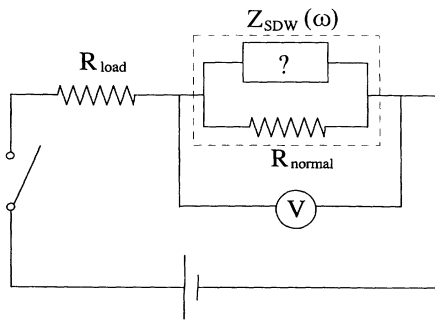

FIG. 2. The equivalent circuit which was used to analyze the data from the discharging experiments. The sample, inside the dashed box, was modeled as a parallel connection of an Ohmic resistor, representing the normal electron contribution, and an unknown frequency-dependent impedance for the SDW contribution.

ear conduction.

In the frequency range from 10^2 to 10^6 Hz, the discharging current density following an electric field step was measured. After the step, in an open circuit configuration, the discharging of the sample produced a time decay of the sample voltage, which was amplified and displayed on a digital oscilloscope. Since the Ohmic part of the sample resistance is frequency independent below 1 MHz, the measured voltage divided by the dc resistance of the sample gives the discharge current $j(t)$ of the polarized SDW. One can determine both components of the complex SDW conductivity using

$$\hat{\sigma}_{\text{SDW}}(\omega) = i\omega \int_0^\infty \left[\frac{j(t)}{E_0}\right] e^{-i\omega t} dt, \qquad (2)$$

where E_0 is the size of the applied electric field during the pulse.[48] The frequency limitation with this technique is determined by the rise time of the voltage amplifier, which in our measurements was 1 μs.

Above 1 kHz, the ac impedance was measured with a lock-in amplifier. A direct measurement of both the magnitude and phase of the sample voltage to an applied ac current directly gave $\hat{\sigma}(\omega)$. These measurements also provided a cross-check on some of the results from the real time experiments and within the region of frequency overlap; both techniques gave identical results.

To investigate $\hat{\sigma}(\omega)$ in the radio-frequency range, above 4 MHz, an HP 8754A network analyzer was used. In this technique, an unknown impedance is determined by measuring the complex reflectance $\hat{r}$ from a shunted transmission line. For a line impedance Z_{line} of 50 Ω and a sample impedance of $\hat{Z}$, the complex reflectance is given by

$$\hat{r} = \frac{\mathbf{E}_{\text{refl}}}{\mathbf{E}_{\text{in}}} = \frac{\hat{Z} - Z_{\text{line}}}{\hat{Z} + Z_{\text{line}}}, \qquad (3)$$

where $\mathbf{E}_{\text{in}}$ and $\mathbf{E}_{\text{refl}}$ are the incident and reflected electric fields at the boundary, respectively. The transmission line was shunted by mounting the sample with Ag paste to 10 μm Au wires which were in turn attached to the open end of a coaxial cable. The rf signal from the network analyzer was split and directed into both a reference and sample arm by an HP 8502A reflection test set. The signal reflected from the sample arm was mixed with the signal from the reference arm at the network analyzer. Both the magnitude and the phase of the resulting signal were recorded with a digital oscilloscope. The linearity of the response was checked by varying the power output with a calibrated step attenuator (0 to -70 dB) while simultaneously monitoring both the magnitude and phase of the signal. For all incident power levels, the reflected power varied linearly with the incident power while the phase remained constant. A finite path difference between the reference and sample arms was intentionally introduced to produce a periodic variation of the phase as the frequency was swept between 4 and 1300 MHz, thus providing a calibration of the source frequency.

The sample was cooled while monitoring the two probe dc resistance and no signs of sample cracking were observed. Furthermore, by subtracting a temperature in-

dependent contact resistance of 1.3 Ω, excellent quantitative agreement was found with the four probe measurements (see Fig. 1) over the entire temperature range (2–300 K).

In order to calibrate the reflectance of the network analyzer, both a shorted and open-ended sample arm were first measured ($\hat{r}= -1$ and 1 respectively). The normalized sample reflectance at each frequency was determined by comparing to the calibrated points. The frequency dependence of the measured magnitude and phase of the normalized sample reflectance exhibited an oscillatory behavior with a well-defined period of nearly 106 MHz. These oscillations, which also appeared in the calibration data, are due to standing waves within the sample arm, with a period corresponding to twice the optical length of the arm. A correction procedure was used which fit the oscillations with a frequency-independent reflectance of nearly 10%. The resultant signal displayed the slow variation of the frequency-dependent reflectance due to the sample.

The measured reflectance $\hat{r}$ determined the impedance of both the sample and the contact. Assuming a simple, purely resistive, serial connection

$$\hat{Z} = \hat{Z}_{\text{sample}} + R_{\text{contact}}, \tag{4}$$

where the value of R_{contact} was determined from the temperature-dependent dc resistance measurement. $\hat{Z}_{\text{sample}}$ was modeled as a parallel connection of a frequency-dependent resistor $R_{\text{sample}}(\omega)$ and capacitor $C_{\text{sample}}(\omega)$,

$$\frac{1}{\hat{Z}_{\text{sample}}} = \frac{1}{R_{\text{sample}}(\omega)} + i\omega C_{\text{sample}}(\omega). \tag{5}$$

Using the measured sample length l and cross sectional area A, the real and imaginary parts of the conductivity were calculated using

$$\sigma_1(\omega) = \frac{1}{R_{\text{sample}}(\omega)} \frac{l}{A}, \tag{6}$$

$$\sigma_2(\omega) = \omega C_{\text{sample}}(\omega) \frac{l}{A}. \tag{7}$$

The final results in the low temperature SDW state are consistent both with the calibrations made and also with reflectance of the sample in the normal state, where it can be simply regarded as a constant known Ohmic resistance.

B. Experiments in the micro- and millimeter wave spectral range

In order to measure $\hat{\sigma}(\omega)$ in the micro- and millimeter wave range, we employed a cavity perturbation technique using resonant cavities which span nearly two orders of magnitude in frequency. Cylindrical cavities in the TE$_{011}$ mode which resonate at $f_0=7$, 9, 12, 35, 60, 100, and 150 GHz were used, together with a split ring resonator at 3 GHz similar to that described in Ref. 49.

The experimental setup und measurement technique are discussed in detail in Ref. 50. The micro- or millimeter wave power was supplied by either a broadband Impatt source or Gunn oscillator and guided with rectangular waveguide to an input coupling hole on the top plate of the cavity. A crystal detector mounted atop a second waveguide measured the power transmitted through the cavity. Both the source and detector were matched to the transmission line with ferrite isolators to avoid standing waves. A broadband mixer, attached to the reference arm of a 10 dB directional coupler, was connected to an EIP model No. 578 microwave-frequency counter. An in-line modulator chopped the microwave signal, allowing for lock-in detection techniques. Finally, a Mylar window atop each stainless steel waveguide was used to ensure a vacuum tight environment. A small amount of He exchange gas was used to provide a weak thermal link to the He bath. A complete temperature sweep from 1.5 K to 300 K was possible and at each desired temperature, both the width Γ and frequency f_0 of the cavity resonance were measured. A Lorentz fit to the resonance line shape was made by sweeping the frequency through the resonance, with the resulting fit giving both Γ and f_0. However, with typical Q's on the order of 10^4, a frequency sweep of at least several hundred kHz was required to fit the base line. Such a large frequency sweep made it difficult to accurately determine the resonant frequency.

In order to obtain a precise measurement of both Γ and f_0, we have developed a feedback technique which locks the source to the resonance frequency. (This technique cannot be easily employed for cavities in the reflection mode, and therefore at 7, 9, and 12 GHz we used a method similar to that described above.) In this, the so-called amplitude technique, the source frequency is swept over a very narrow range about f_0, which is constantly tracked by feeding the derivative of the signal back to the source as a frequency correction. This allows a precise tracking of the resonance frequency as the temperature varies. Furthermore, the transmission signal is modulated and measured with a second lock-in amplifier. For a Lorentzian response,

$$P(f_0)\Gamma^2 = \text{const}, \tag{8}$$

where $P(f_0)$ is the amplitude of the transmitted signal at f_0 and the constant only depends on the total power emitted by the source. As the microwave power is independent of the cavity temperature, the constant is temperature independent and can be evaluated at room temperature, where both the amplitude and the width can be carefully measured. Thus, by measuring $P(f_0)$ and f_0 versus temperature, we are able to determine the temperature dependence of both the width and the resonant frequency.

In all cases, the sample conductivity $\hat{\sigma}$ is related to the change in the cavity parameters, $\Delta\Gamma$ and Δf, caused by the introduction of the sample into the cavity. Experiments were conducted by first measuring the temperature dependence of Γ and f_0 of the empty cavity followed by a subsequent measurement of the same parameters with the sample inside the cavity. Using the method

described above, we reduced the measurement error to $\delta(\Delta\Gamma/2f_0) \approx 3 \times 10^{-7}$ and $\delta(\Delta f/f_0) \approx 3 \times 10^{-7}$ at room temperature, with a further factor of 2 improvement at low temperature.[51]

For specimens where the skin depth $\delta = \sqrt{2/\mu_0\omega\sigma_1}$ is smaller than the sample dimensions (a condition obeyed by most of the samples we investigated), the parameter which determines the change of the resonance characteristics upon insertion into the cavity is the surface impedance

$$\hat{Z}_s = R_s + iX_s = \left(\frac{i\mu_0\omega}{\sigma_1 - i\sigma_2}\right)^{1/2}, \tag{9}$$

where R_s and X_s are the surface resistance and surface reactance, respectively and μ_0 is the permeability of free space. In this, the so-called skin-effect (or surface impedance) regime, R_s is proportional to the excess loss and, consequently, to the change in width $\Delta\Gamma/2f_0$ caused by the sample while X_s is proportional to the frequency shift $\Delta f/f_0$ from an identically shaped perfect conductor, or

$$\frac{\Delta f}{f_0} = \frac{f_s - f_0}{f_0} - C = \frac{\xi X_s}{Z_0}, \tag{10}$$

$$\frac{\Delta\Gamma}{2f_0} = \frac{1}{2}\left(\frac{1}{Q_s} - \frac{1}{Q_0}\right) = \frac{\xi R_s}{Z_0}, \tag{11}$$

where the constant C includes the perfect conductor shift together with an unreproducible frequency shift which occurs when the cavity is opened in order to insert the sample, ξ is a geometrical constant which depends on the dimensions of both the cavity and the specimen under investigation,[52] and Z_0 is the impedance of free space (377 Ω).

Two different configurations were employed to measure the ac response along the highly conducting direction of the crystals. In one configuration, the sample was placed on the bottom of the cavity near the half-radius point, at the maximum magnetic field $\mathbf{H}_{ac}$, and oriented such that the field was perpendicular to the highly conducting axis. The eddy currents, due to $\mathbf{H}_{ac}$, are mainly along the highly conducting direction, with current flow perpendicular to the chains only near the ends of the specimen. Due to the long, needle-shaped crystals (the highly conducting axis is parallel to the long axis), the contributions due to currents at the ends are expected to be small, and consequently both R_s and X_s should primarily be determined by the conductivity along the chain direction. Alternatively, the specimen was placed on a dielectric post in such a way that the maximum electric field $\mathbf{E}_{ac}$ was parallel to the highly conducting axis. In this configuration $\sigma_1(\omega)$ along the chain direction was measured along with only a very small contribution expected from depolarization currents at the ends of the specimens. We were not able to evaluate the effects associated with the ends of the specimens. However, similar results were obtained for both configurations (the current distributions in the two cases are not the same), strongly suggesting that R_s and X_s were determined by the con-

ductivity along the chain direction. Furthermore, similar results were obtained for specimens with different length to cross section ratios, again indicating that depolarization and/or end effects did not play a significant role.

The resonator constant ξ which appears in Eqs. (10) and (11) has been calculated for an ellipsoidal sample placed at either the maximum electric or magnetic field[52,53] and a very strong dependence on the sample depolarization factor was found. This strong dependence on the sample geometry makes it difficult to precisely determine ξ on irregularly shaped samples and therefore we normally determined the resonator constant using the following procedure. In the metallic state, well above T_{SDW}, if the single particle relaxation rate $1/(2\pi\tau)$ significantly exceeds the measurement frequency, the experiments are performed in the so-called Hagen-Rubens limit $\omega\tau \ll 1$. In this limit $\sigma_1 \gg \sigma_2$ and $\sigma_1 \simeq \sigma_{dc}$. Consequently, from Eq. (9)

$$R_s = X_s = \left(\frac{\mu_0\omega}{2\sigma_{dc}}\right)^{1/2}. \tag{12}$$

Using σ_{dc} as an input parameter, ξ can be evaluated from Eq. (11) and subsequently C can also be determined using Eq. (10). All of these parameters are temperature independent, neglecting corrections due to thermal expansion, and therefore do not change at the phase transition. Nevertheless, the uncertainty concerning the evaluation of C has led us to alternative ways of evaluating or modeling the frequency dependent response, as discussed below in Sec. III. It should also be pointed out that at 7, 9, and 12 GHz, the cavity size is sufficiently large to allow the sample to be rotated in and out of the cavity on a Teflon platform. In this way, the offset associated with the end plate removal can be avoided, but the reproducibility of the rotation then directly determines the sensitivity of Δf.[52]

At low temperatures, where the conductivity is small, the skin depth δ can become comparable to or larger than the minimum sample dimensions. In contrast to the skin-effect regime, the excess loss due to the sample is no longer proportional to R_s. In this, the so-called depolarization regime, a completely different analysis is required in order to extract $\hat{\sigma}$ from the measured parameters. This analysis is discussed in detail in Ref. 52. Here we will only discuss results taken at temperatures where the surface impedance formalism is still valid.

A typical experimental result obtained at 60 GHz is displayed in Fig. 3, where both R_s and X_s are shown together with $\sqrt{\mu_0\omega\rho_{dc}/2}$. In a metal with $\omega\tau < 1$, $R_s = X_s \propto \sqrt{\rho_{dc}}$ [see Eq. (12)] and both R_s and $\sqrt{\rho_{dc}}$ should exhibit the same temperature dependence. Such behavior has been observed above T_{SDW} as shown in Fig. 3. The transition to the SDW state is also visible in Fig. 3, and it is clear that below T_{SDW}, R_s and X_s are no longer equal, indicating a frequency-dependent conductivity. In this case, the measured values of $\hat{Z}_s(T)$ can be inserted into Eq. (9) to evaluate $\hat{\sigma}(T)$ below T_{SDW}. However, at most frequencies, source fluctuations, sample thermal expansion, and small relative effects make it exceptionally difficult to accurately measure X_s. This
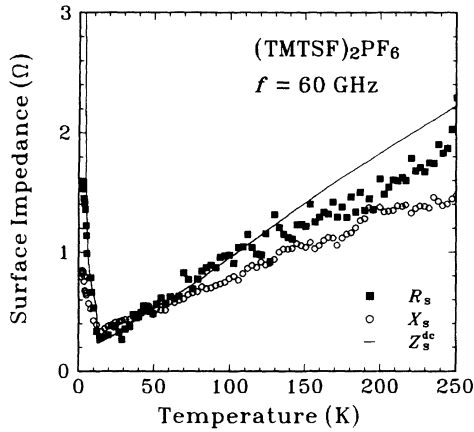
FIG. 3. Temperature dependence of R_s and X_s in $(TMTSF)_2PF_6$ at 60 GHz. Z_s^{dc} is the 60 GHz surface impedance obtained using Eq. (12).

leaves only one measured parameter, R_s, and thus precludes a direct evaluation of σ_1 and σ_2 using Eq. (9).

We display the measured surface resistance at various frequencies in Figs. 4(a) and 4(b), where we have plotted $2R_s^2/\mu_0\omega$ in order to compare with the dc resistivity. Data, such as displayed in the figures, have been
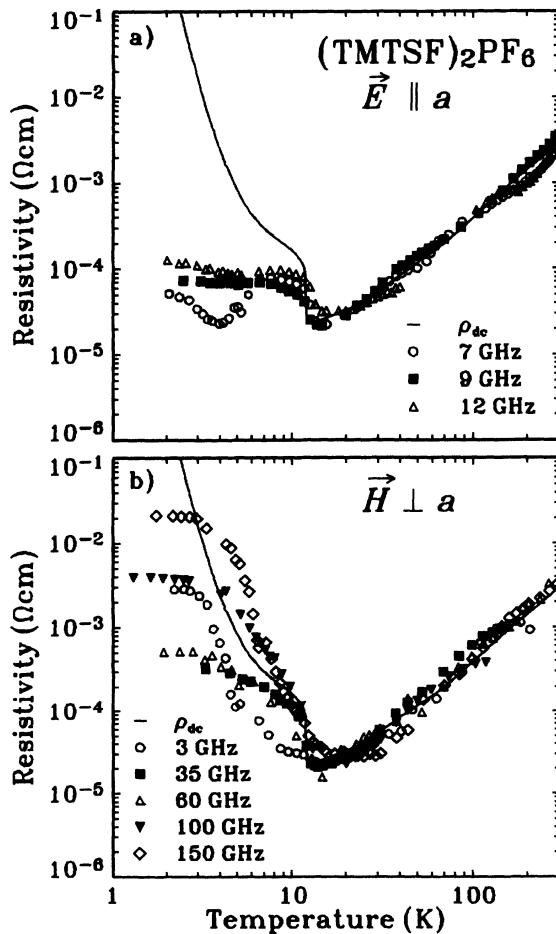

FIG. 4. Temperature dependence of the microwave resistivity $2R_s^2/\mu_0\omega$ at various frequencies. Results are shown from measurements made in both the electric (a) and magnetic (b) field antinodes.
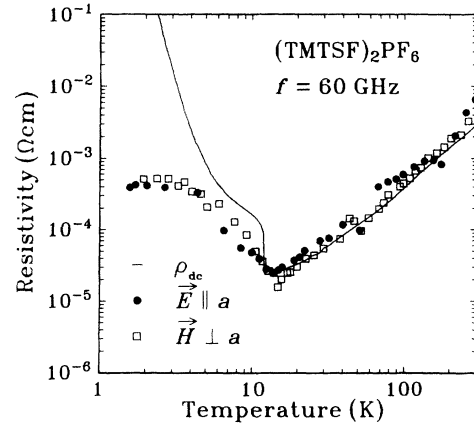

FIG. 5. A comparison of the microwave resistivity $2R_s^2/\mu_0\omega$ of a single crystal measured in both the electric and magnetic field antinodes.

obtained in several specimens and were generally reproducible during both cooling and warming. Furthermore, at the same frequency nearly identical results were obtained in both the electric and magnetic field antinodes, as shown in Fig. 5, strongly indicating that the measurements in both configurations probe the conductivity along the same crystal direction. The agreement between both microwave measurements and the a-axis dc resistivity in the metallic state indicates that it is the a-axis conductivity which is probed by the microwaves. We believe the results presented in Figs. 4(a) and 4(b) represent the intrinsic behavior of R_s along the highly conducting axis in $(TMTSF)_2PF_6$.

Our experimental results obtained at 9 GHz are displayed in Fig. 6 together with our earlier results[23,25] and those obtained by other groups.[22,24] Although there is some discrepancy at low temperatures (most likely due to the strong dependence of the pinned mode on the residual impurity concentration), all the measured data unam-
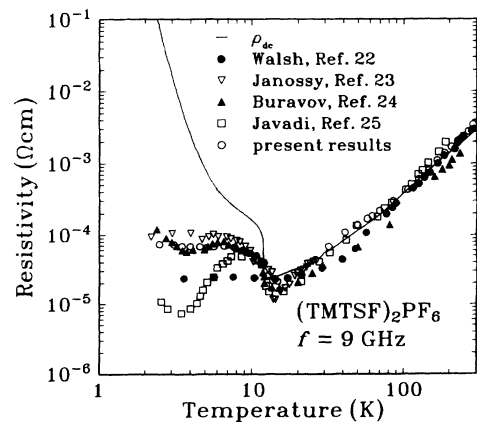

FIG. 6. The 9 GHz microwave resistivity of $(TMTSF)_2PF_6$ as measured by several different groups. Earlier results from Walsh *et al.* (Ref. 22), Jánossy *et al.* (Ref. 23), Buravov *et al.* (Ref. 24), and Javadi *et al.* (Ref. 25) are compared with the present results.

biguously show a strongly frequency-dependent response in the microwave wave spectral range.

C. Optical experiments

Reflectance measurements on mosaics of $(TMTSF)_2PF_6$ have been performed from the far infrared (FIR) (20–600 cm^{-1}) up to the midinfrared (MIR) (500–5500 cm^{-1}) spectral range using a Bruker IFS 113v fast scan Fourier transform interferometer. A Hg arc light source was used in the FIR in conjunction with either a He$_{4.2 K}$ or a He$_{1.2 K}$ cooled Infrared Laboratory Si bolometric detector. Several measurements were made using different Mylar beam splitters (thickness 125, 50, 12, and 6 μm, respectively) and the relevant data with each beam splitter were combined. In the MIR spectral range, a Globar source and KBr beam splitter were used with an MCT$_{77 K}$ detector. The samples were placed in an Oxford cryostat with polyethylene (FIR) and KRS 5 (MIR) windows. In both spectral ranges, measurements of the sample reflectivity $R(\omega)$ were made at several temperatures both above and below T_{SDW} (i.e., at 2, 5, 10, 20, 40, and 300 K), with a freshly evaporated gold mirror used as a reference. The experiments were made with light polarized both parallel and perpendicular to the chain direction. In the following, unless stated otherwise, we will always refer to the parallel direction.

Due to the small crystal size, measurements had to be performed on mosaics, which were obtained by aligning three to five single crystals along the chain axis. We built four different mosaics from as many different sample batches. In order to facilitate the alignment procedure, particular care was taken in choosing only those needles having a large, smooth, rectangularly shaped surface (0.5–1 mm in width and 3–4 mm long). The samples were then mounted on a 3 mm diameter Cu ring and fixed with a small amount of five minute epoxy. Due to the fragility of the samples, we cooled the mosaics slowly (with a typical cooling rate of about 0.3 K/min). With the exception of the one mosaic which was destroyed upon cooling, no visual damage to the samples was observable and all results were reproducible. In order to correct for any spurious scattering from the irregular surface of the mosaic, a 1500 Å layer of Ag was deposited on the mosaic after the initial set of measurements and the entire measurement procedure was repeated on the Ag coated mosaic.

The absorptivity, $A(\omega) = 1 - R(\omega)$, in the FIR is shown in the inset of Fig. 7(a) at 5 K. Besides a broad dip near 100 cm^{-1}, which was slightly enhanced in one run, the overall absorptivity is rather structureless. As seen in the inset, our FIR results agree quantitatively (within 2% in reflectivity) with previous measurements made using a bolometric technique.[54] At higher frequencies, we have made a simple interpolation of our data to the measurements made previously from the MIR up to the visible spectral range[55] and the resulting absorptivity is shown in Fig. 7(a). One of the most important results of this investigation is the temperature independence of the reflectivity spectra in the FIR from 2 to 300 K, which is also in full agreement with several
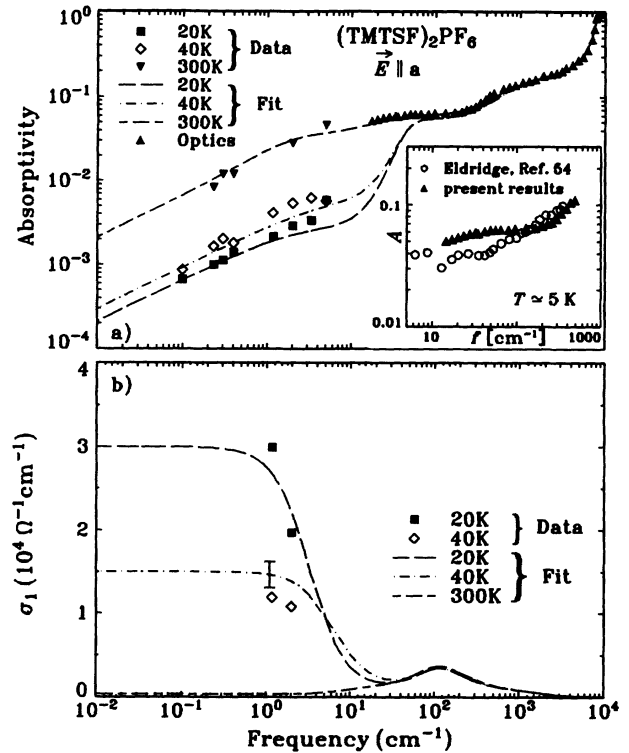

FIG. 7. (a) The absorptivity of $(TMTSF)_2PF_6$ at 20 K. Both the surface impedance and optical results are shown on the figure. The lines are fits to the measured data using both a Drude and harmonic oscillator fit (parameters given in the text). In the inset, the optical data is compared with a previous measurement on the same compound made by Eldridge and Bates (Ref. 54). (b) The optical conductivity $\sigma_1(\omega)$ at 20 K, 40 K, and 300 K as evaluated from a Kramers-Kronig transformation of the data in (a).

other previous investigations.[56,57] The consequences of this large temperature-independent feature will be discussed in detail later.

III. ANALYSIS AND DISCUSSION

We first discuss the procedures which are used to convert the measured data into $\hat{\sigma}(\omega)$, followed by an analysis of the results in both the normal and SDW states. Several different models are briefly mentioned which describe the frequency-dependent response in both the metallic and SDW states and finally a comparison between theory and experiment is made.

A. Data analysis

So far we have presented several different types of measured data obtained with a large variety of techniques. At low frequencies, up through the rf, two parameters were experimentally accessible and hence both the real and imaginary parts of the $\hat{\sigma}$ were directly determined.

On the other hand, at higher frequencies only one experimental parameter was directly accessible [R_s in the micro- and millimeter spectral range and the reflectivity $R(\omega)$ in the optical spectral range]. In order to combine the micro- and millimeter wave data together with the optical results, we have adopted the following procedure. The surface impedance $\hat{Z}_s(\omega)$ is given by

$$\hat{Z}_s(\omega) = \sqrt{\frac{\mu_0}{\epsilon_0}} \frac{1}{\hat{N}} = \frac{Z_0}{\hat{N}}, \tag{13}$$

where $\hat{N} = \sqrt{\hat{\epsilon}}$ is the complex refractive index, and $\hat{\epsilon} = \epsilon_\infty + i\hat{\sigma}/(\epsilon_0\omega)$ is the complex dielectric constant. The reflectivity is given by

$$R(\omega) = \left| \frac{1 - \hat{N}}{1 + \hat{N}} \right|^2. \tag{14}$$

The relationship between R_s, X_s, and $R(\omega)$ can be calculated from Eqs. (13) and (14), giving

$$R(\omega) = 1 - \frac{4R_s}{Z_0} \left(1 + \frac{2R_s}{Z_0} + \frac{R_s^2 + X_s^2}{Z_0^2} \right)^{-1}. \tag{15}$$

In the limit $R_s, X_s \ll Z_0$, the higher order terms in Eq. (15) can be neglected, yielding

$$A(\omega) = 1 - R(\omega) = \frac{4R_s}{Z_0}. \tag{16}$$

Thus, in this limit, the absorptivity is directly proportional to only R_s. As Z_0 is very large (compare with the measured values of the surface impedance displayed in Fig. 3), the limit is appropriate for most of the situations we intended to examine.

In order to obtain $\hat{\sigma}(\omega)$, a Kramers Kronig (KK) transformation[58] was performed on the reflectivity, as determined by both optical and micro- and millimeter wave techniques. The conductivity is given by

$$\sigma_1(\omega) = \epsilon_0\omega \frac{4\sqrt{R(\omega)}[1 - R(\omega)]\sin\Theta}{[1 + R(\omega) - 2\sqrt{R(\omega)}\cos\Theta]^2}, \tag{17}$$

$$\sigma_2(\omega) = \epsilon_0\epsilon_1\omega = \epsilon_0\omega \frac{[1 - R(\omega)]^2 - 4R(\omega)\sin^2\Theta}{[1 + R(\omega) - 2\sqrt{R(\omega)}\cos\Theta]^2}, \tag{18}$$

where the phase $\Theta(\omega)$ is obtained from

$$\Theta(\omega') = \frac{\omega'}{\pi} \int_0^\infty \frac{\ln[R(\omega)] - \ln[R(\omega')]}{\omega'^2 - \omega^2} d\omega. \tag{19}$$

As the integral in Eq. (19) extends from zero to infinity, one must use suitable frequency extrapolations to the measured data. We used a power law high frequency extrapolation [$R(\omega) \propto 1/\omega^3$] and a Hagen-Rubens extrapolation [$R(\omega) \approx 1 - \sqrt{8\omega\epsilon_0/\sigma_{dc}}$] at low frequency. In spite of the fact that Eq. (19) is nonlocal, changes in the absorptivity turn out to have primarily a local influence on the output, and we found that neither the low nor high frequency extrapolations significantly affected the KK results in the FIR, and vice versa.

B. Sum rule

The well-known optical sum rule[58]

$$\int_0^\infty \sigma_1(\omega)d\omega = \frac{\epsilon_0\omega_p^2\pi}{2} = \frac{\pi n_{tot}e^2}{2m_e}, \tag{20}$$

where ω_p is the plasma frequency, n_{tot} the total electron density, e the electronic charge, and m_e the electronic mass, relates the measured spectral weight to the n_{tot}/m_e ratio and is valid in all systems irrespective of particle interactions or magnetic field and at any temperature. A limiting form of Eq. (20) considers only electrons in a particular band and in this case the integral is proportional to the ratio n/m_b, where n and m_b are the electron density and band mass, respectively. Furthermore, if absorption peaks within the band are well separated, an n/m ratio can be loosely associated with each absorption peak. At any phase transition, the total spectral weight is conserved,

$$\int_0^\infty \sigma_1(\omega, \text{above } T_c)d\omega = \int_0^\infty \sigma_1(\omega, \text{below } T_c)d\omega, \tag{21}$$

although the various contributions together with their relative weight may change. For a transition to either a superconducting or density wave ground state one finds

$$\int_0^\infty \sigma_1(\omega)d\omega = \sum_{\text{collective mode}} \int_0^\infty \sigma_1^{cm}(\omega)d\omega + \sum_{\text{single particle}} \int_0^\infty \sigma_1^{sp}(\omega)d\omega, \tag{22}$$

and both the collective mode [$\sigma_1^{cm}(\omega)$] and single particle excitations [$\sigma_1^{sp}(\omega)$] make contributions to the total spectral weight.

C. Metallic state

Above T_{SDW}, the dc conductivity and other transport properties of (TMTSF)$_2$PF$_6$ clearly indicate a metallic

ground state. A simple Drude model gives

$$\hat{\sigma}(\omega) = \epsilon_0\omega_p^2 \frac{\tau}{1 - i\omega\tau} = \frac{ne^2\tau}{m_b} \frac{1}{1 - i\omega\tau} = \frac{\sigma_{dc}}{1 - i\omega\tau}, \tag{23}$$

where the plasma frequency $\omega_p = [ne^2/(\epsilon_0 m_b)]^{1/2}$. With a dc conductivity $\sigma_{dc} = ne^2\tau/m_b = 3.0 \times 10^4$ (Ω cm)$^{-1}$ at $T = 20$ K, a carrier concentration of $n = 1.4 \times 10^{21}$ cm^{-3}

(corresponding to a complete charge transfer), and a band mass $m_b \approx 3m_e$, as calculated from magnetic susceptibility,[4-6,59] the simple Drude description leads to a relaxation rate of $1/(2\pi\tau)$=17.5 cm^{-1}=520 GHz. This description, however, may not be appropriate for several reasons. First, it has been suggested[60] that these materials may not be described in terms of a simple Drude model. The evidence for this view comes from optical measurements conducted on a variety of organic linear-chain compounds. These measurements indicate the formation of a narrow resonance centered at zero frequency.[61] In terms of a renormalized Drude response, this would lead to a strongly increased relaxation time τ' [i.e., corresponding to a $1/(2\pi\tau')$ of about 0.3 cm^{-1}, (Ref. 54)], and at the same time to a strongly enhanced effective mass m' or strongly reduced carrier density n'. The behavior, as implied from the optical studies, is not understood, as the magnetic susceptibility[4-6] does not show strong deviations from a simple metallic behavior. Another problem may arise from the small bandwidth in these compounds; intraband transitions with a significant oscillator strength may occur at relatively low frequencies.

The absorptivity above T_{SDW} is displayed in Fig. 7(a) at 20 K. A fit to the data (dashed line) was made by modeling the dielectric response in terms of a Drude contribution plus two harmonic oscillators,

$$\hat{\epsilon}(\omega) = \epsilon_1(\omega) + i\epsilon_2(\omega)$$
$$= \epsilon_\infty - \frac{\omega_p^2}{\omega^2 + i\omega/\tau} + \sum_{i=1}^{2} \frac{\omega_{pi}^2}{\omega_i^2 - \omega^2 + i\omega\gamma_i} , \quad (24)$$

where $\omega_p/2\pi$=2450 cm^{-1} and $1/(2\pi\tau)$=3.3 cm^{-1} are the plasma frequency and damping of the free electrons and ω_i, γ_i, and ω_{pi} are the frequency, damping, and mode strength of the harmonic oscillators, respectively: $\omega_{p1}/2\pi$=9333 cm^{-1}, $\gamma_1/2\pi$= 1433.3 cm^{-1}, $\omega_1/2\pi$= 117 cm^{-1}, and $\omega_{p2}/2\pi$=5333 cm^{-1}, $\gamma_2/2\pi$=200 cm^{-1}, $\omega_2/2\pi$= 117 cm^{-1}, and $\epsilon_\infty = 2$ is the high frequency dielectric constant contribution. The fits shown at 40 K, and 300 K were made only by varying the Drude scattering rate $1/(2\pi\tau)$ [$1/(2\pi\tau)$=3.3 cm^{-1} at 20 K, 6.67 cm^{-1} at 40 K, and 333 cm^{-1} at 300 K]. The dc conductivity found from using these scattering rates is in full agreement with the increase measured in the dc resistivity between 300 K and 20 K.

The complete excitation spectrum obtained by a straightforward KK analysis is shown in Fig. 7(b) at 20 K, 40 K, and 300 K. We observe that the zero frequency limit of $\sigma_1(\omega)$ is in good agreement with the values obtained from the dc transport measurements. At room temperature the conductivity is quite structureless. On the contrary, at 20 K, $\sigma_1(\omega)$ shows a rapid decrease above approximately 1 cm^{-1} before merging with the broad temperature-independent tail at higher frequencies. However, at all temperatures, from the FIR up to the optical energy spectral range, $\sigma_1(\omega)$ is dominated by the broad temperature-independent feature centered near 100 cm^{-1}. Furthermore, at all temperatures the total spectral weight, determined by integrating un-

der the curve in Fig. 7(b), corresponds to the previously observed[55] plasma frequency of $\Omega_p/2\pi = 10^4$ cm^{-1}.

The hump observed near 100 cm^{-1} is quite similar to a feature observed near 50 cm^{-1} in $(\mathrm{TMTSF})_2\mathrm{AsF}_6$.[62] This feature was previously explained as optical evidence of the SDW gap and the occurrence of this absorption at a frequency close to the gap $2\Delta/h$, determined from dc transport measurements, strongly supported such an interpretation. It was also found that this feature persists above T_{SDW}, indicating the presence of a pseudogap as a consequence of fluctuation effects.[57] However, previous investigations on mosaics have failed to show such a sharp feature[56,57,61,63] and the broad and continuous absorption in the 50–500 cm^{-1} region was associated with a Holstein process (i.e., a photon is absorbed, with the simultaneous creation of an electron-hole pair and a phonon) by other groups[56,61,63] Our experimental findings show the temperature independence of this feature up to 300 K, and this essentially rules out any relationship with the single particle gap. At the moment, the origin of this hump is not understood, but it may be related to an intraband transition.

At both 35 and 60 GHz it is possible to directly measure $\hat{\sigma}$ and the values obtained in this way at both 20 K and 40 K are displayed in Fig. 7(b). These values are in good agreement with the results obtained from the KK analysis. The 20 K Drude scattering rate, $1/(2\pi\tau)$, that we find (3.3 cm^{-1}) is almost two orders of magnitude smaller than the value extracted from a previous optical investigation [240 cm^{-1} (Ref. 55)]. However, this is not surprising due to the large feature which exists in the FIR. A Drude plasma frequency of only 2500 cm^{-1} implies that only 6% of the total spectral weight resides with the Drude contribution; the remaining 94% is associated with the temperature-independent feature. Such a small spectral weight implies an enhanced bandmass of m_b=20m_e ($n = 1.4 \times 10^{21}$ cm^{-3} from simple counting arguments). This value is somewhat higher than the value obtained from susceptibility measurements [$m_b \approx 3m_e$ (Refs. 4–6)], but both measurements point to a mild enhancement.

D. Spin-density wave state

Below T_{SDW}, the resistivity of $(\mathrm{TMTSF})_2\mathrm{PF}_6$ displays an activated behavior up through the audio- and radiofrequency range of the spectrum (up to about 1 GHz).[64] However, such a strong temperature dependence is not seen for data taken in the microwave range of frequencies (7, 9, 12 GHz). In particular, one can see from Figs. 4(a) and 4(b), that the quantity $2R_s^2/\mu_0\omega$ is much less affected by the transition to the SDW state in the microwave range of frequencies (7, 9, and 12 GHz) than in the millimeter wave spectral range (35, 60, 100, and 150 GHz). Such behavior is indicative of a strongly frequency-dependent response. However, we must caution the reader that $2R_s^2/\mu_0\omega$ is only proportional to the resistivity in the limit $\sigma_1 \gg \sigma_2$, and this condition is not fulfilled in the region near a narrow resonance.

For this reason, we followed the procedure as outlined previously and display the measured absorptivity below

the SDW transition in Fig. 8(a). The optical results were found to be independent of temperature and unaffected by the transition to the SDW state. For the sake of completeness, we have also included the results obtained at 5 and 10 K in Fig. 8(b). The optical conductivity obtained from the KK transform is displayed in Fig. 8(c). A resonance at temperatures below T_{SDW} is clearly evident near 0.1 cm^{-1}. This resonance was formerly identified[33] as the pinned mode resonance. The single particle gap $2\Delta/h= 30$ cm^{-1}, as established from the temperature de-
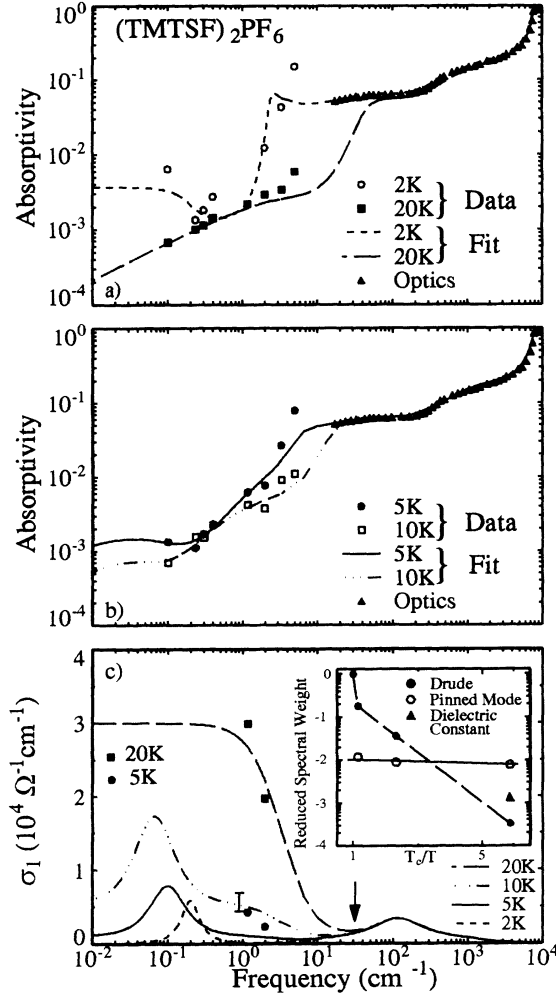

FIG. 8. (a) The frequency dependence of the absorptivity both above ($T=20$ K) and below T_{SDW} ($T=2$ K) in (TMTSF)$_2$ PF$_6$. The surface impedance measurements and the optical results are shown (symbols) together with a simple harmonic oscillator fit (lines). (b) The absorptivity at 5 and 10 K. (c) The frequency-dependent conductivity both above and below T_{SDW} as determined from a Kramers-Kronig analysis of (a) and (b). The single particle gap $2\Delta/h$ at 30 cm^{-1}, obtained from dc measurements, is indicated with an arrow. In the inset, the temperature dependence of the normalized spectral weight (normalized to the spectral weight of the Drude response at 20 K) of the various contributions to $\sigma_1(\omega)$ below T_{SDW} is displayed. Also shown is the spectral weight of the pinned mode at 2 K as determined from the dielectric constant.

pendence of the dc conductivity, is also indicated on the figure with an arrow. Previously,[33] we have associated the increase of $\sigma_1(\omega)$ around this frequency with the gap in the SDW state, but the temperature independence of this feature seems to rule this possibility out. In fact, the absence of a gap structure in the optical conductivity is not surprising in light of the fact that these materials are in the clean limit. This phenomenon is identical to that found in many superconductors; in the clean limit, $\sigma_1(\omega)$ is small in the spectral range around 2Δ, and consequently the effect of the removal of this spectral weight leads to only slight changes in the reflectivity.

A small increase in the frequency of this resonance can be seen as the temperature is lowered and we attribute this to the reduction in the number of normal carriers available to screen the interaction with the impurities. The temperature dependence of the spectral weight of this resonance was evaluated by fitting the observed conductivity with a function of the form

$$\hat{\sigma}(\omega)= \hat{\sigma}_{sp}(\omega) + \hat{\sigma}_{SDW}(\omega)$$

$$= \frac{n(T)e^2\tau}{m_b(1 - i\omega\tau)} - \frac{i\epsilon_0 f'(T)\omega_p^2\omega}{[(\omega_0^2 - \omega^2) - i\omega/\tau^*]}, \quad (25)$$

where the first term $\hat{\sigma}_{sp}$ is the Drude response of the thermally excited electrons, the second $\hat{\sigma}_{SDW}$ is the Lorentzian term which describes the resonance, $n(T)$ is the number of uncondensed electrons (determined from the temperature dependence of σ_{dc} below the transition), and $f'(T)$ is the fraction of the spectral weight associated with the condensate. Here, we have followed the convention previously used to successfully describe the frequency-dependent response of a CDW,[1-3,65] and within this convention ω_0 is the pinning frequency, and m^* and τ^* represent the effective mass and damping associated with the condensate. A temperature-independent τ has been used for $T < T_{SDW}$. The spectral weight associated with the two contributions in Eq. (25) is displayed in the inset of Fig. 8(c) as a function of temperature. It is clear from the figure that in contrast to the temperature-dependent Drude contribution, $f'(T)$ is only weakly temperature dependent below T_{SDW}, with a value near 10^{-2}. This strong reduction of the spectral weight has been independently confirmed at $T = 2$ K by a measurement of the low frequency dielectric constant ϵ_1.[34] It is apparent from the inset of Fig. 8(c) that, at low temperatures, most of the spectral weight previously associated with the Drude response does not appear under the SDW excitation. One might be tempted to associate it with the gap, but we have no experimental evidence for doing so. In fact, due to the large temperature-independent feature in the FIR, this "missing" spectral weight represents only 6% of the total spectral weight ($\epsilon_0\Omega_p^2\pi/2$ where Ω_p is 10^4 cm^{-1}). Several suggestions have been made as to the origin of this missing spectral weight and we will discuss these later.

The detailed form of the low lying resonance was explored by combining the optical data with experiments in the radio-frequency spectral range. In the inset of Fig. 9 we display $\hat{\sigma}_{SDW}(\omega)$ for (TMTSF)$_2$PF$_6$, together
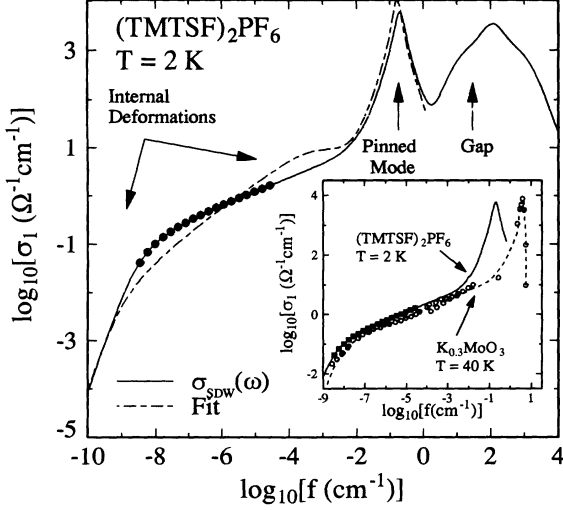
FIG. 9. The real part of the SDW conductivity $\hat{\sigma}_{\mathrm{SDW}}(\omega)$ at 2 K is displayed. The internal deformations, the pinned mode, and the temperature-independent feature are all clearly visible. Using the theory of a weakly pinned Fröhlich mode (Ref. 69), we fit the conductivity using the following parameters: $\omega_{\mathrm{LO}}/2\pi$=3.5 cm^{-1}, f'=0.0083, $\gamma_0/2\pi$=0.084 cm^{-1}, $\omega_r/2\pi = 5.3 \times 10^{-4}$ cm^{-1}, $\omega_w/2\pi$=0.20 cm^{-1}, $\epsilon_{1,\Delta} = 4.6 \times 10^3$, $\omega_0/2\pi = 0.2$ cm^{-1}, and $\epsilon_1(0)$=1.1$\times 10^9$. In the inset, we compare the SDW conductivity $\hat{\sigma}_{\mathrm{SDW}}(\omega)$ for (TMTSF)$_2$PF$_6$ with the CDW conductivity $\hat{\sigma}_{\mathrm{CDW}}(\omega)$ found in K$_{0.3}$MoO$_3$. The measured conductivity is shown (symbols) together with the output of the Laplace transform of the polarizability (lines). In each case, the measurements shown were made well below the transition temperature.

with $\hat{\sigma}_{\mathrm{CDW}}(\omega)$ observed[2,3] in K$_{0.3}$MoO$_3$. In both cases we find a broad structure at low frequencies together with a well-defined resonance in the high frequency end of the structure. In the CDW system the low frequency behavior has been analyzed in detail and is now well understood[2,3,65] to be due to the internal deformations of the collective mode. Furthermore, the resonance which appears at 100 GHz for K$_{0.3}$MoO$_3$ is usually referred to as the pinned mode resonance at the frequency ω_0 and it is due to $q = 0$ oscillations of the condensate. Extensive experiments[1] on several materials with a CDW ground state have clearly established that ω_0 is determined by pinning to the impurities, and that it represents the oscillations of the entire collective mode subject to an average restoring force whose spring constant is given by $K = m^*\omega_0^2$. Much less is known about the electrodynamical response of the SDW materials. Experiments on SDW samples with varying impurity concentrations are currently underway in order to determine the dependence of $\sigma_1(\omega)$ on impurity concentration (although still incomplete, these experiments[66] indicate a behavior similar to that seen in a variety of CDW compounds). The striking similarity of the frequency-dependent response of these two systems strongly suggests that the low frequency mode in (TMTSF)$_2$PF$_6$ is due to internal deformations of the SDW and the mode around 0.1 cm^{-1} is

the response of the pinned SDW. All of the different excitations of the condensate are clearly displayed in Fig. 9, where we summarize our results on the electrodynamic response of (TMTSF)$_2$PF$_6$ at T=2 K.

Finally, a previous investigation has found evidence of the so-called phase phonons in the optical response of (TMTSF)$_2$SbF$_6$ below T_{SDW}.[61] These infrared active modes are due to the coupling of a CDW with intramolecular phonons, and they appear as sharp excitations in $\sigma_1(\omega)$.[67] In a SDW ground state they are unexpected (since the dominant interaction is the electron-electron and not the electron-phonon one like in the CDW ground state). Nevertheless, it was believed that they might appear as a consequence of the second order CDW induced by the SDW. If true, this would provide evidence for a coupling to the lattice. However, our investigation does not give any evidence for such phase phonons, in agreement with bolometric measurements.[54,57]

1. Frequency-dependent response in the SDW state

The dynamics of the SDW state are determined by the relative magnitudes of the parameters 2Δ, τ, and ω_0. In contrast to superconductors, impurities give rise to SDW pair breaking, and this leads to a suppression of the transition temperature T_{SDW}. This is given by[68]

$$-\ln\left(\frac{T_{\mathrm{SDW}}}{T_{\mathrm{SDW}}^0}\right) = \Psi\left(\frac{1}{2}+\rho\right) - \Psi\left(\frac{1}{2}\right), \qquad (26)$$

where $\rho = (\Gamma_1 + \Gamma_2/2)/(2\pi T_{\mathrm{SDW}})$ with Γ_1 and Γ_2 the forward scattering and backscattering rates, respectively, T_{SDW}^0 the transition temperature in the absence of impurities, and Ψ the digamma function. In the model[68] where Eq. (26) is derived, $\Gamma_2 < \Gamma_1$ and $\tau = (2\Gamma_2)^{-1}$. Consequently, the SDW transition approaches zero as $\tau\Delta/\hbar$ approaches unity, and within the framework of the approximations[68] the dirty limit cannot be achieved. To express this in a different way, in order to have T_{SDW} for an "impure" system close to T_{SDW}^0, the condition $\tau\Delta/\hbar \gg 1$ has to be obeyed. This is clearly the case for the specimens investigated by us. As a brief estimate from Eq. (26), we find that for $T_{\mathrm{SDW}}/T_{\mathrm{SDW}}^0 \geq 0.9$ (a situation roughly corresponding to the experimental resolution concerning the transition temperature of various specimens from the same batch) $\tau\Delta/\hbar \geq 20$. For (TMTSF)$_2$PF$_6$ near the transition the relaxation time evaluated from the dc conductivity $\sigma_{\mathrm{dc}} = ne^2\tau/m_b \approx 3 \times 10^4$ $(\Omega\,\mathrm{cm})^{-1}$ with $n = 10^{21}$ cm^{-3} and $m_b = 20m_e$ is given by $1/(2\pi\tau) \approx 3.0$ cm^{-1} and consequently with $2\Delta/h = 30$ cm^{-1}, $\hbar/\tau \ll 2\Delta$, placing the material well into the clean limit, in agreement with the conclusion reached above. For $\hbar/\tau \ll 2\Delta$, the relevant parameters which determine the response are ω_0 and 2Δ, and the situation for $\omega_0 < 2\Delta/\hbar$ is shown schematically in Fig. 10. For $\omega < 2\Delta/\hbar$, the pinned mode contribution dominates the response, with a small residual contribution at $\omega > 2\Delta/\hbar$ coming from single particle excitations. This latter contribution vanishes in the extreme clean limit, $1/\tau \to 0$. In the opposite limit $\omega_0 \gg 2\Delta/\hbar$,
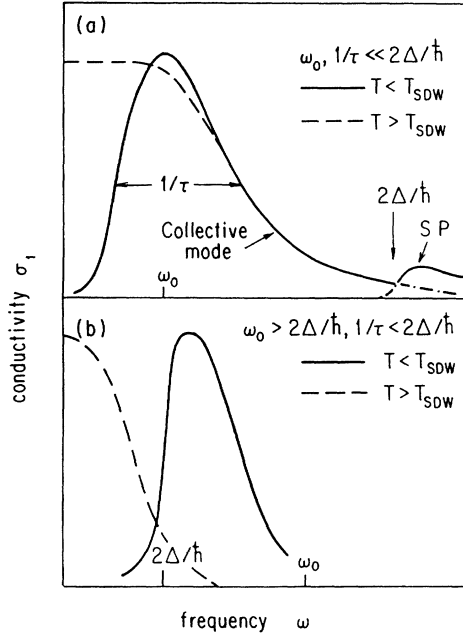
FIG. 10. (a) Expected $\sigma_1(\omega)$ both above and below the SDW transition in the clean limit with $\hbar\omega_0 \ll 2\Delta$. SP refers to the single particle response of electrons excited across the gap. (b) The same plot but in the limit $\hbar\omega_0 \gg 2\Delta$.

single particle excitations appear at lower energy, with the phason contribution dominant at higher frequencies. The expected frequency-dependent response is displayed in Fig. 10 for the two limits. Such a model neglects any contributions from the internal modes and also assumes that all the spectral weight associated with the Drude rate in the metallic phase appears under either the pinned mode or single particle excitations in the SDW state. Within such a model, the dielectric constant, in the dc (i.e., $\omega \to 0$) limit, is given by

$$\epsilon_1(0) = 1 + \frac{f'(T)\omega_p^2}{\omega_0^2} + \frac{[1 - f'(T)]\hbar^2\omega_p^2}{6\Delta^2}, \quad \omega_0 \ll 2\Delta/\hbar,$$

(27)

$$\epsilon_1(0) = 1 + \frac{\hbar^2\omega_p^2}{\Delta^2}, \quad \omega_0 \gg 2\Delta/\hbar,$$

(28)

where the second term in Eq. (27) is the contribution of the pinned collective mode, the last term in each equation is due to single particle excitations, and $f'(T)$ is the fraction of the spectral weight associated with the condensate.

The internal modes play an important role in the dynamics of the CDW, leading to a strongly enhanced conductivity and dielectric constant at low frequency.[1] The same is true for the SDW, and neglecting the internal modes in Eq. (27) leads to a serious discrepancy with the measured dielectric constant. Using the values obtained in the microwave range at $T = 2$ K, $f' \approx 10^{-2}$, $\omega_0/2\pi \approx 0.2$ cm^{-1}, $\omega_p/2\pi \approx 2500$ cm^{-1}, and

$2\Delta/\hbar \approx 30$ cm^{-1}, in Eq. (27) gives a nearly frequency-independent value, in the limit $\omega \ll \omega_0$, of $\epsilon_1(0) = 10^6$. The measured value of $\epsilon_1(\omega)$ is shown in Fig. 11,[34] and there are two important points to notice: First, the low frequency value exceeds 10^9 (even larger than that found in materials with a CDW ground state) and second, it is strongly frequency dependent in the region below the pinned mode. For the sake of completeness, we have included the value obtained only by fitting the microwave data, neglecting the internal modes, and it is shown in the inset. In fact the measured dielectric constant can be used to set an upper limit to the value of the spectral weight associated with the pinned mode and the procedure is as follows: Any contribution to ϵ_1 from the pinned mode must be frequency independent in the region well below the pinned mode resonance, and therefore from Fig. 11 it is clear that such a contribution cannot exceed 2×10^5. Using this value in Eq. (27) together with the measured values of ω_0 and ω_p at 2 K gives a value of 1.3×10^{-3} for $f'(T = 2$ K). This value is shown in the inset of Fig. 8(c) and provides an independent confirmation that the spectral weight is strongly reduced in the pinned mode.

In order to quantitatively characterize the pinned mode resonance and the frequency region below, where the internal SDW deformations interact with screening quasiparticles via random impurity pinning,[36] we will apply the theory of Ref. 69 to the measured SDW conductivity, as displayed in Fig. 9. In an extended Fukuyama-Lee-Rice description of the phason dynamics, the SDW conductivity $\sigma_{SDW}(\omega)$ can be approximated by Eq. (12) in Ref. 69 in the limit $\omega \ll \Delta/\hbar$ with weak anisotropic pinning in three spatial dimensions. Within this description, there are several physical quantities which can be estimated from the present measurements.
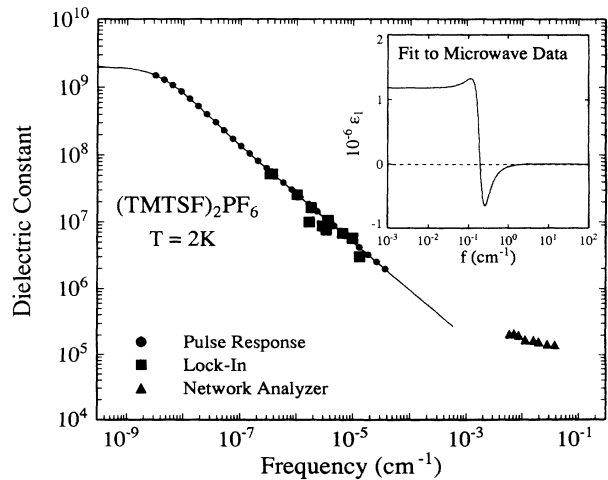

FIG. 11. The dielectric constant is shown at 2 K in (TMTSF)$_2$PF$_6$. The response to a voltage pulse is shown together (solid circles and line) with results from both a lock-in amplifier and a network analyzer. In the inset, the dielectric constant corresponding to the fit of the measured micro- and millimeter wave data is shown.

We adopt the notion of a SDW with a strongly reduced spectral weight f'. Below we will comment on possible reasons for such a reduction. In the present case, Fig. 8(c) shows that $f' \approx 10^{-2}$. The frequency-dependent version of Eq. (27) predicts for $\omega_0^2 \ll 6f'\Delta^2 \ll \omega_p^2$, two frequencies of longitudinal oscillations, namely, ω_p and $\omega_{LO} = \omega_p(f'/\epsilon_{1,\Delta})^{1/2} \ll \omega_p$, where $\epsilon_{1,\Delta} = \hbar^2\omega_p^2/6\Delta^2 \gg 1$ is the dielectric constant associated with the SDW gap. The lower frequency mode, ω_{LO}, is the frequency of the longitudinal optical phason and it is not directly seen in the electromagnetic response. However, ω_{LO} has a strong influence[69,36] on the response of the collective mode for frequencies below ω_0, in the region where a harmonic oscillator description fails.

This frequency region is characterized by a low frequency relaxation mode seen in ϵ_2 around a frequency ω_{peak} and a power law shoulder between ω_{peak} and ω_0 seen in σ_1. The frequency ω_{peak} is proportional to (though much smaller than) the dielectric relaxation frequency of the quasiparticles, $\omega_r = 4\pi\sigma_{dc}/\epsilon_{1,\Delta}$.[70,71] The relaxation mode is manifested in Fig. 9 by the downturn of σ_1 near 10^{-8} cm^{-1}. The relaxation mode also marks a broad transition region in $\epsilon_1(\omega)$ from the huge static dielectric constant $\epsilon_1(0)$ to a plateau value $\epsilon_1^* = f'\omega_p^2/\omega_0^2$. Using the measured values of $\omega_p/2\pi = 2500$ cm^{-1} and $\omega_0/2\pi = 0.20$ cm^{-1}, one obtains an ϵ_1^* of 1.3×10^6 at $T = 2$ K.

In Fig. 9, a fit of the theory to the measured collective mode response was made using the following parameters: Longitudinal optical phason $\omega_{LO}/2\pi = 3.5$ cm^{-1}, spectral weight factor $f' = 0.0083$, bare phason damping rate $\gamma_0/2\pi = 0.084$ cm^{-1}, dielectric relaxation frequency of quasiparticles $\omega_r/2\pi = 5.3 \times 10^{-4}$ cm^{-1}, Lee-Rice weak pinning scale frequency $\omega_w/2\pi = 0.20$ cm^{-1}, gap dielectric constant $\epsilon_{1,\Delta} = 4.6 \times 10^3$, and a static dielectric constant $\epsilon_1(0) = 1.1 \times 10^9$. These values coincide, at least to the order of magnitude, with those from the present experiments. The measured data are thus consistent with the view that the collective mode in (TMTSF)$_2$PF$_6$ has a strongly reduced spectral weight.

Presently, we can only speculate on the origin of the missing spectral weight in the SDW state. According to Eq. (22), there must be excitations associated with the SDW response in addition to those found in the microwave region and below. The temperature independence of this mode seems to rule out the Anderson-Higgs mechanism,[41] as it would lead to an exponential freeze-out of the spectral weight of the pinned mode resonance with decreasing temperature. One likely explanation is that the missing spectral weight is associated with bound states accompanying the SDW condensate.[65] In contrast to CDW's, it is expected that bound states due to impurities can readily occur, and the reasoning is as follows: In a CDW the periodically modulated charge density can adjust to the electrostatic impurity potentials by adjusting its local phase to minimize the total energy (electrostatic + elastic) gain. On the other hand, the SDW ground state can be viewed as two CDW's, one for each spin direction, with a CDW modulation on the sublattices which differs by π. As the pinning in a SDW is also due to electrostatic forces,[36] a full adjustment of the phase cannot occur simultaneously for both spin sublattices, leaving a net energy gain which is much larger than that for a CDW. However, the electrostatic energy can be lowered by removing electrons from the condensate to form a bound state about the impurity. In addition, the spectral weight of these bound states is expected to be significantly larger than in CDW systems. The spatial extension of a bound state is given by the coherence length $\xi_0 = \frac{\hbar v_F}{\pi\Delta}$, and with a Fermi velocity $v_F = 10^7$ cm/s, and single particle gap $\Delta/h = 30$ cm^{-1}, $\xi_0 = 10^3$ Å, which is significantly larger than the coherence length for typical CDW systems. As the matrix element for the optical transition of the bound state is proportional to its dipole moment and hence to ξ_0, a large coherence length leads to a large optical spectral weight associated with that transition.

An alternate model[43] suggests that as these materials are near to commensurability, soliton excitations could occur below the gap. These excitations would also have a large spectral weight. At the present, we do not have clear spectroscopic evidence for states below the single particle gap, but a detailed study of the submillimeter range is currently underway. Furthermore, since the missing spectral weight is much smaller ($\approx 6\%$) than that associated with the temperature-independent feature above the gap, we cannot experimentally determine whether the missing weight is above or below the continuum of single particle excitations.

IV. CONCLUSION

In conclusion, we have presented our measurements made on the compound (TMTSF)$_2$PF$_6$ in both the metallic and SDW states. The normal state properties are characterized by a simple Drude type behavior at low frequency together with a large temperature-independent feature in the FIR. At temperatures just above T_{SDW}, (TMTSF)$_2$PF$_6$ is in the clean limit. Below the phase transition, a strongly frequency-dependent conductivity has been found. Both internal mode deformations and oscillations of the condensate have been observed. The spectral weight of the pinned mode resonance is strongly reduced, implying either a large effective mass or small number of relevant excitations. The reason for such a small spectral weight is not understood at the present, but the frequency-dependent conductivity can be fit quite well within an extended Fukuyama-Lee-Rice model of phason dynamics.

ACKNOWLEDGMENTS

† Permanent address: Laboratorium für Festkörperphysik Eidgenössische Technische Hochschule (HPF-F3) CH-8093 Zürich Switzerland.

[1] G. Grüner, Rev. Mod. Phys. **60**, 1129 (1988).

[2] L. Degiorgi, B. Alavi, G. Mihály, and G. Grüner, Phys. Rev. B **44**, 7808 (1991).

[3] L. Degiorgi and G. Grüner, Phys. Rev. B **44**, 7820 (1991).

[4] K. Mortensen, Y. Tomkiewicz, T. D. Schultz, and E. M. Engler, Phys. Rev. Lett. **46**, 1234 (1981).

[5] K. Mortensen, Y. Tomkiewicz, and K. Bechgaard, Phys. Rev. B **25**, 3319 (1982).

[6] J. B. Torrance, H. J. Pedersen, and K. Bechgaard, Phys. Rev. Lett. **49**, 881 (1982).

[7] T. Takahashi, Y. Maniwa, H. Kawamura, K. Murata, and G. Saito, Synth. Met. **41-43**, 225 (1987).

[8] D. Jérome, F. Creuzet, and C. Bourbonnais, Phys. Scr. **T27**, 130 (1989).

[9] L. P. Le *et al.*, Europhys. Lett. **15**, 547 (1991).

[10] J. M. Delrieu, M. Roger, Z. Toffano, A. Moradpour, and K. Bechgaard, J. Phys. (Paris) **47**, 839 (1986).

[11] J. M. Delrieu, M. Roger, Z. Toffano, E. Wope Mbougue, P. Fauvel, R. Saint James, and K. Bechgaard, Physica **143B**, 412 (1986).

[12] E. Barthel, G. Quirion, P. Wzietek, D. Jérome, J. B. Christensen, M. J. Jorgensen, and K. Bechgaard, Europhys. Lett. **21**, 87 (1993).

[13] T. Ishiguro and K. Yamaji, *Organic Superconductors* (Springer-Verlag, Berlin, 1990).

[14] P. A. Lee, T. M. Rice, and P. W. Anderson, Solid State Commun. **14**, 703 (1974).

[15] A. Zawadowski and I. Tüttö, Synth. Met. **29**, F469 (1989).

[16] P. F. Tua and J. Ruvalds, Phys. Rev. B **32**, 4660 (1985).

[17] A. Virosztek and K. Maki, Phys. Rev. B **37**, 2028 (1988).

[18] I. Tüttö and A. Zawadowski, Phys. Rev. Lett. **60**, 1442 (1988).

[19] K. Maki and A. Virosztek, Phys. Rev. B **39**, 2511 (1989).

[20] S. Takada, J. Phys. Soc. Jpn. **53**, 2193 (1984).

[21] P. M. Chaikin, G. Grüner, E. M. Engler, and R. L. Greene, Phys. Rev. Lett. **45**, 1874 (1980).

[22] W. M. Walsh, Jr., F. Wudl, G. A. Thomas, D. Nalewajek, J. J. Hauser, P. A. Lee, and T. Poehler, Phys. Rev. Lett. **45**, 829 (1980).

[23] A. Jànossy, M. Hardiman, and G. Grüner, Solid State Commun. **46**, 21 (1983).

[24] L. I. Buravov, V. N. Laukhin, and A. G. Khomenko, Zh. Eksp. Teor. Fiz. **88**, 2185 (1985) [Sov. Phys. JETP **61**, 1292 (1985)].

[25] H. H. S. Javadi, S. Sridhar, G. Grüner, L. Chiang, and F. Wudl, Phys. Rev. Lett. **55**, 1216 (1985).

[26] S. Tomić, J. R. Cooper, D. Jérome, and K. Bechgaard, Phys. Rev. Lett. **62**, 462 (1989).

[27] S. Tomić, J. R. Cooper, W. Kang, and D. Jérome, Synth. Met. **41-43**, 4007 (1991).

[28] G. Kriza, G. Quirion, O. Traetteberg, W. Kang, and D. Jérome, Phys. Rev. Lett. **66**, 1922 (1991).

[29] N. Hino, T. Sambongi, K. Nomura, M. Nagasawa, M. Tokumoto, H. Anzai, N. Kinoshita, and G. Saito, Synth. Met. **40**, 275 (1991).

[30] G. Kriza, Y. Kim, and G. Mihály, Phys. Rev. B **45**, 1466 (1992).

[31] W. H. Wong, M. E. Hanson, B. Alavi, W. G. Clark, and W. A. Hines, Phys. Rev. Lett. **70**, 1882 (1993).

[32] J. M. Delrieu and N. Kinoshita, Synth. Met. **41-43**, 3947 (1991).

[33] D. Quinlivan, Y. Kim, K. Holczer, G. Grüner, and F. Wudl, Phys. Rev. Lett. **65**, 1816 (1990).

[34] G. Mihály, Y. Kim, and G. Grüner, Phys. Rev. Lett. **66**, 2806 (1991).

[35] P. B. Littlewood (private communication).

[36] P. B. Littlewood, Phys. Rev. B **36**, 3108 (1987).

[37] H. Fukuyama (private communication).

[38] E. W. Fenton and G. C. Psaltakis, Solid State Commun. **47**, 767 (1983).

[39] E. W. Fenton and G. C. Aers, in *Low-Dimensional Conductors and Superconductors*, edited by D. Jérome and L. Caron (Plenum, New York, 1987), p. 285.

[40] J. P. Pouget, R. Moret, R. Comes, K. Bechgaard, J. M. Fabre, and L. Giral, Mol. Cryst. Liq. Cryst. **79**, 129 (1982).

[41] K. Maki and G. Grüner, Phys. Rev. Lett. **66**, 782 (1991).

[42] P. W. Anderson, *Frontiers in Physics: Basic Notions of Condensed Matter Physics* (Benjamin-Cummings, Menlo Park, CA, 1984), Vol. 55.

[43] W. Wonneberger, Solid State Commun. **80**, 953 (1991).

[44] S. Donovan, Y. Kim, L. Degiorgi, and G. Grüner, J. Phys. (France) I **3**, 1493 (1993).

[45] S. Donovan, L. Degiorgi, and G. Grüner, Europhys. Lett. **19**, 433 (1992).

[46] G. Grüner, Synth. Met. **41-43**, 3767 (1991).

[47] K. Bechgaard, C. S. Jacobsen, K. Mortensen, H. J. Pedersen, and N. Thorup, Solid State Commun. **33**, 1119 (1980).

[48] V. V. Daniel, *Dielectric Relaxation* (Academic Press, London, 1967).

[49] D. A. Bonn, D. C. Morgan, and W. N. Hardy, Rev. Sci. Instrum. **62**, 1819 (1991).

[50] S. Donovan, O. Klein, M. Dressel, K. Holczer, and G. Grüner, Int. J. Infrared Millimeter Waves **14**, 2459 (1993).

[51] M. Dressel, O. Klein, S. Donovan, and G. Grüner, Int. J. Infrared Millimeter Waves **14**, 2489 (1993).

[52] O. Klein, S. Donovan, M. Dressel, and G. Grüner, Int. J. Infrared Millimeter Waves **14**, 2423 (1993).

[53] M. Cohen, S. K. Khanna, W. J. Gunning, A. F. Garito, and A. J. Heeger, Solid State Commun. **17**, 367 (1975).

[54] J. E. Eldridge and G. S. Bates, Mol. Cryst. Liq. Cryst. **119**, 183 (1985).

[55] C. S. Jacobsen, D. B. Tanner, and K. Bechgaard, Phys. Rev. B **28**, 7019 (1983).

[56] H. K. Ng, T. Timusk, D. Jérome, and K. Bechgaard, Phys. Rev. B **32**, 8041 (1985).

[57] K. Kornelsen, J. E. Eldridge, and G. S. Bates, Phys. Rev. B **35**, 9162 (1987).

[58] F. Wooten, *Optical Properties of Solids* (Academic Press, San Diego, 1972).

[59] Using the measured value of χ at $T = 20$ K in a free electron gas model, one obtains $m_b/m_e \approx 3$.

[60] T. Timusk, in *Organic Superconductors*, edited by V. Z. Kresin and W. A. Little (Plenum Press, New York, 1990), and references therein.

[61] H. K. Ng, T. Timusk, and K. Bechgaard, Phys. Rev. B **30**, 5842 (1984).

[62] J. E. Eldridge and G. S. Bates, Phys. Rev. B **34**, 6992 (1986).

[63] C. S. Jacobsen, D. B. Tanner, and K. Bechgaard, Mol. Cryst. Liq. Cryst. **79**, 25 (1982).

[64] A. Zettl, G. Grüner, and E. M. Engler, Phys. Rev. B **25**, 1443 (1982).

[65] L. Degiorgi and G. Grüner, Europhys. Lett. **16**, 97 (1991).

[66] S. Donovan, A. Schwartz, M. Dressel, O. Traetteberg, R. Gáal, and G. Grüner (unpublished).

[67] M. J. Rice, Phys. Rev. Lett. **37**, 36 (1976).

[68] K. Maki, Phys. Rev. B **41**, 9308 (1990).

[69] W. Wonneberger, Synth. Met. **41-43**, 3793 (1991).

[70] R. J. Cava, R. M. Fleming, P. B. Littlewood, E. A. Riet-man, L. F. Schneemeyer, and R. G. Dunn, Phys. Rev. B **30**, 3228 (1984).

[71] G. Mihály, T. W. Kim, and G. Grüner, Phys. Rev. B **39**, 13009 (1989).